Available online at www.sciencedirect.com

ScienceDirect

IFAC PapersOnline CONFERENCE PAPER ARCHIVE

IFAC PapersOnLine 58-5 (2024) 28–33

Noise-induced chaos in an electronic Burridge-Knopoff model analog

Alessio Perinelli [*,**,***] **Roberto Iuppa** [*,**] **Leonardo Ricci** [*]

[*] *Department of Physics, University of Trento, 38123 Trento (Italy).*
[**] *INFN-TIFPA, University of Trento, 38123 Trento (Italy).*
[***] *(e-mail: alessio.perinelli@unitn.it)*

Abstract: Electronic analog circuits are valuable platforms to experimentally address physical systems whose implementation would otherwise be unwieldy. Besides validating numerical predictions, electronic analogs of nonlinear systems are also ideal tools to study the effect of noise injection in realistic conditions and are often more scalable than numerical approaches. In this work, we address the effect of noise injection in an electronic analog of the Burridge-Knopoff mechanical model of earthquake faults. Noise is injected into the friction term of the mechanical system: interestingly, the presence of a sufficient level of noise can trigger the onset of chaos in otherwise periodic regimes.

Copyright © 2024 The Authors. This is an open access article under the CC BY-NC-ND license (https://creativecommons.org/licenses/by-nc-nd/4.0/)

Keywords: eletronic analog; control of bifurcation and chaos; chaotic circuit; noise; Burridge-Knopoff model;

1. INTRODUCTION

The Burridge-Knopoff (BK) model is a mechanical description of the interface between two plates in an earthquake fault (Burridge and Knopoff, 1967; Carlson et al., 1994). The model approximates plate elasticity by means of a chain of discrete massive blocks that are mutually coupled through springs. External driving is provided by an upper ceiling that moves at constant velocity and is elastically coupled to the blocks also via springs. The surface on which the blocks move exerts a nonlinear, velocity-dependent friction. As a consequence, each block behaves as a stick-slip oscillator (Popp and Stelter, 1990), and the coupling of as few as two blocks yields a rich dynamics that exhibits chaotic regimes (Ryabov and Ito, 1995; de Sousa Vieira, 1999).

A valuable strategy to experimentally investigate the dynamics of the BK model, whose direct physical implementation would be unwieldy, consists of implementing an electronic analog of the system. The first implementation, demonstrated by Field et al. (1995), confirmed the existence of chaos, despite the proposed circuit has several drawbacks and does not allow to tune the system's parameters. More recently, an improved electronic analog of the BK model was developed by Perinelli et al. (2023) with the explicit purpose to maximize tunability and scalability.

The improved electronic analog is here exploited to study the effect of noise injection in the BK model. Specifically, white noise with normally distributed amplitudes is superimposed to a voltage parameter that determines the functional shape of the nonlinear friction analog. The voltage parameter was kept constant in the pristine model.

This paper is organized as follows. The mechanical system and its electronic analog are summarized in Sec. 2. The experimental investigation of noise injection is the topic of Sec. 3. Concluding remarks and perspectives are outlined in Sec. 4.

2. BURRIDGE-KNOPOFF MODEL AND ITS ELECTRONIC ANALOG IMPLEMENTATION

A diagram of the two-blocks mechanical BK model is shown in Fig. 1. The blocks of mass m are coupled together

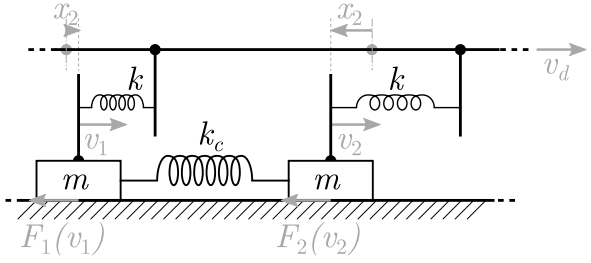

Fig. 1. Diagram of the mechanical BK model with two blocks.

by a spring of elastic constant k_c and each one is coupled, by means of springs of elastic constant k, to an upper ceiling that moves at a constant velocity v_d. Blocks are initially at rest ("stick"). The upper ceiling "loads" the system by providing a slow, constant external driving that produces a stress accumulation in the k springs: when the force acting on a block overcomes a threshold, the block slides ("slip"), possibly triggering the sliding of the other block by virtue of the k_c spring. The resulting stick-slip behavior is reminiscent of the slow stress accumulation and sudden release observed in real faults. A crucial ingredient to sustain this oscillatory behavior–also known as stick-slip vibration (Popp and Stelter, 1990)–is the nonlinear, velocity-dependent friction $F(v)$ exerted by the surface on the blocks.

2405-8963 Copyright © 2024 The Authors. This is an open access article under the CC BY-NC-ND license.
Peer review under responsibility of International Federation of Automatic Control.
10.1016/j.ifacol.2024.07.059

To mathematically describe the dynamics, each block is described in terms of its displacement x_i–in the ceiling's frame–with respect to the unperturbed position of the k springs. Conversely, velocities are measured in the surface frame, whereby the ceiling moves with a constant velocity v_d. For two blocks, the equations of motion are:

$$\begin{aligned} m\dot{v}_1 &= -kx_1 - k_c(x_1 - x_2) - F(v_1)\,, \\ \dot{x}_1 &= v_1 - v_d\,, \\ m\dot{v}_2 &= -kx_2 - k_c(x_2 - x_1) - F(v_2)\,, \\ \dot{x}_2 &= v_2 - v_d\,. \end{aligned}$$

The velocity-dependent friction $F(v)$ is a monotonically decreasing function of velocity (Nakanishi, 1998): a typical choice is that of an hyperbolic dependence (Carlson, 1991) given, for example, by $F(v) = F_0 \frac{(1-\sigma)^2}{1-\sigma+v}$, with σ a positive constant typically much less than 1 ($0 < \sigma \ll 1$). Furthermore, the blocks are prevented to move backwards or, equivalently, always have a non-negative velocity. This constraint is usually formalized by setting $F(v) \to -\infty$ when $v < 0$. The model described so far contains only two blocks, but a generalization to N blocks is straightforward. Similarly, one can expand the model from a one-dimensional chain to a two-dimensional lattice, where a block is connected to its four nearest neighbors—two for each direction (Nakanishi, 1998).

A possible strategy to devise an electronic analog of the system is that of following the so-called impedance analogy or the complementary admittance analogy (Bertuccio, 2022). The latter procedure was followed by Field et al. (1995), who proposed the first electronic analog, and indeed the first experimental implementation, of the BK model. The resulting circuit (see Fig. 1 of Field et al. (1995)) relies on inductors to simulate elastic couplings and capacitors to mimick masses. Consequently, voltages turn to correspond to velocities and currents, once multiplied by the related inductances, to positions. To implement friction, a nonlinear resistive element made of two complementary junction field-effect transistors (JFET) was used (Chua et al., 1985).

Despite its elegance, this analogy bears several drawbacks. The presence of inductors is the most prominent issue, as these components are bulky, have large tolerances and are hardly tunable. A second issue is the fact that part of the dynamical state is implemented by currents, which are definitely harder to measure than voltages and, in addition, might lead to an excessive power consumption. Finally, the reproducibility and tunability of the friction analog is severly limited by the use of JFETs. All these aspects render the inductor-based circuit hardly scalable, and thus unsuitable to build large-scale electronic analog of the BK model with possibly hundreds or thousands of units.

An alternative approach was proposed by Perinelli et al. (2023), in which the issues listed above were overcome by implementing the system via circuits that merely contain resistors, capacitors, diodes and operational amplifiers (op-amps). The corresponding circuit diagram for a single block is shown in Fig. 2. The voltage signals W_i, V_i, with $i = 1, 2$, are the electronic analog of position x_i and velocity v_i, respectively.

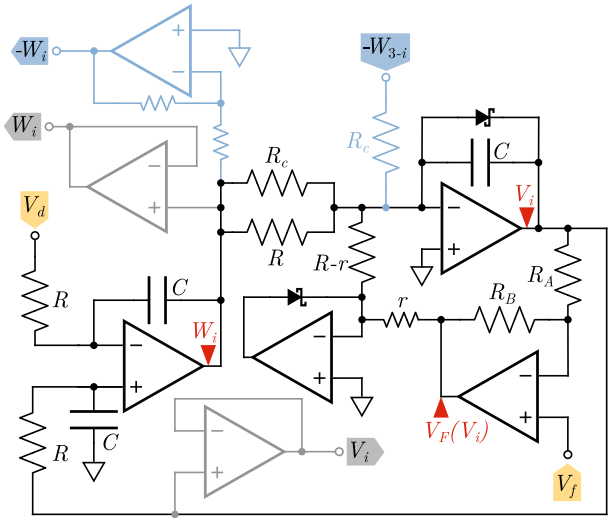

Fig. 2. Diagram of a single block (labeled by i) of the op-amp-based electronic analog BK model. Arrows highlight input and output ports of the block. Gray parts of the circuit correspond to output buffers. Light blue parts correspond to coupling elements with the other block. Yellow inputs correspond to the tunable system's voltage parameters. The voltages corresponding to the state variables W_i, V_i, as well as to the nonlinear friction V_F, are highlighted in red.

A thorough analysis of the circuit's equations and how those were derived from a dimensionless form of the original BK model is discussed by Perinelli et al. (2023). To summarize, the dynamics of two coupled blocks is driven by the following system of integral equations, whose form highlights the action of the op-amp-based integrator networks:

$$\begin{aligned} V_1 + \Delta V &= -\frac{1}{RC}\int \left[(1+\lambda)\,W_1 - \lambda W_2 + V_F\,(V_1)\right]\,\mathrm{d}t\,, \\ W_1 &= -\frac{1}{RC}\int (V_d - V_1)\,\mathrm{d}t\,, \\ V_2 + \Delta V &= -\frac{1}{RC}\int \left[(1+\lambda)\,W_2 - \lambda W_1 + V_F\,(V_2)\right]\,\mathrm{d}t\,, \\ W_2 &= -\frac{1}{RC}\int (V_d - V_2)\,\mathrm{d}t\,, \end{aligned}$$

where $\lambda = R/R_c$ corresponds to the ratio k_c/k in the mechanical system.

The Schottky diode in parallel to the capacitor on the feedback network of V_i's integrator implements the condition of the related block to avoid a negative velocity. As a result, the voltages V_1, V_2 are always non-negative. In the real implementation, however, because of the finite voltage drop across the diode ($V_{\mathrm{diode}} \simeq 0.3\,\mathrm{V}$), this condition can be only fulfilled in a "moving surface reference frame": this is the reason for the ΔV in the equations above, which restores the requirement of non-negative velocities once we set $\Delta V = V_{\mathrm{diode}} \simeq 0.3\,\mathrm{V}$. (See Perinelli et al. (2023) for a more in-depth discussion on this point.)

The nonlinear friction is implemented as a voltage $V_F(V_i)$ produced by the bottom-right op-amp, as follows:

$$V_F(V_i) = \frac{R_A + R_B}{R_A} V_f - \frac{R_B}{R_A} V_i \,.$$

As required by the model, V_F is a monotonically decreasing funcion of V_i. To approximate the hyperbolic friction law mentioned in Sec. 2, an active clamp relying on a Schottky diode on the feedback network of an additional op-amp is connected to the voltage V_F. In this way, V_F is prevented from going negative. In the implementation by Perinelli et al. (2023), $R_A = R_B$, $V_f = 0.5\,\mathrm{V}$, so that the velocity-independent, i.e. "static", component of the friction voltage is a constant equal to 1.0 V. Crucially, in the investigation at hand, V_f is noisy, thus bestowing the static friction a stochastic component.

The system with two blocks implemented as the circuit of Fig. 2 was built by relying on OP470GSZ (Analog Devices, 2002, rev. B) quadruple op-amp chips, DFLS1100 (Diodes Incorporated, 2021, rev. 14-2) Schottky diodes. The settings of the resistive and capacitive components are: $C = 100\,\mathrm{nF}$, $R = R_c = 10\,\mathrm{k\Omega}$, $R_A = R_B = 10\,\mathrm{k\Omega}$, $r = 1.8\,\mathrm{k\Omega}$. The tolerances on resistor and capacitors are 1%, and 10%, respectively. The circuit's time constant is then $RC = 1\,\mathrm{ms}$, which results into an oscillation frequency of a single, uncoupled block between 160 Hz and 200 Hz for $V_d < 1\,\mathrm{V}$ (Perinelli et al., 2023). In the present work, signal acquisition was carried out by means of a MSO7054 oscilloscope (RIGOL Technologies) by setting a sampling frequency of 200 kHz and a resolution of 8-bit. Signals were then downsampled by averaging every 16 consecutive samples, yielding an effective 12-bit resolution at a sampling frequency of 12.5 kHz.

3. INTERMITTEND CHAOS TRIGGERED BY NOISE INJECTION

The evolution of the system when the parameters V_d, V_f are set to 0.10 V, 0.50 V, respectively, is taken as the reference behavior. These parameter values yield a chaotic regime, as displayed by the phase portrait of Fig. 3 (a), demonstrated by relying on embedding techniques (Perinelli and Ricci, 2020; Perinelli et al., 2023).

The parameter V_f is exploited to inject dynamical noise in the system. To this purpose, $V_f(t)$ is set to correspond to a constant offset voltage $V_{f,0}$ superimposed to a stochastic signal,

$$V_f(t) = V_{f,0} + \sigma_f \eta(t) \,,$$

where $\eta(t)$ is a white noise process whose amplitude is distributed according to a standard normal distribution and the parameter σ_f corresponds to the noise voltage amplitude. In practice, the voltage signal $V_f(t)$ was generated by means of the oscilloscope's internal function generator, whose "whiteness" is limited by the generator sample rate of 200 MSa/s, which is however much larger than the typical frequencies of oscillation of the circuit and the acquisition sampling rate.

Given a fixed $V_{f,0}$, the presence or absence of noise can trigger different dynamical regimes. An example of this effect is shown in Fig. 3, where the attractors recorded for three different settings of $V_{f,0}$, σ_f are compared. The first two cases, shown in Fig. 3 (a,b), correspond to a noiseless $V_f(t)$, i.e. when $\sigma_f = 0$: while $V_{f,0} = 0.50\,\mathrm{V}$ (reference behavior) yields a chaotic regime, the value $V_{f,0} = 0.45\,\mathrm{V}$ produces a periodic orbit. However, once a noisy contribution of $\sigma_f = 0.33\,\mathrm{V}$ is added, the evolution becomes irregular, and the related phase space portrait closely resembles the one of the reference behavior. A

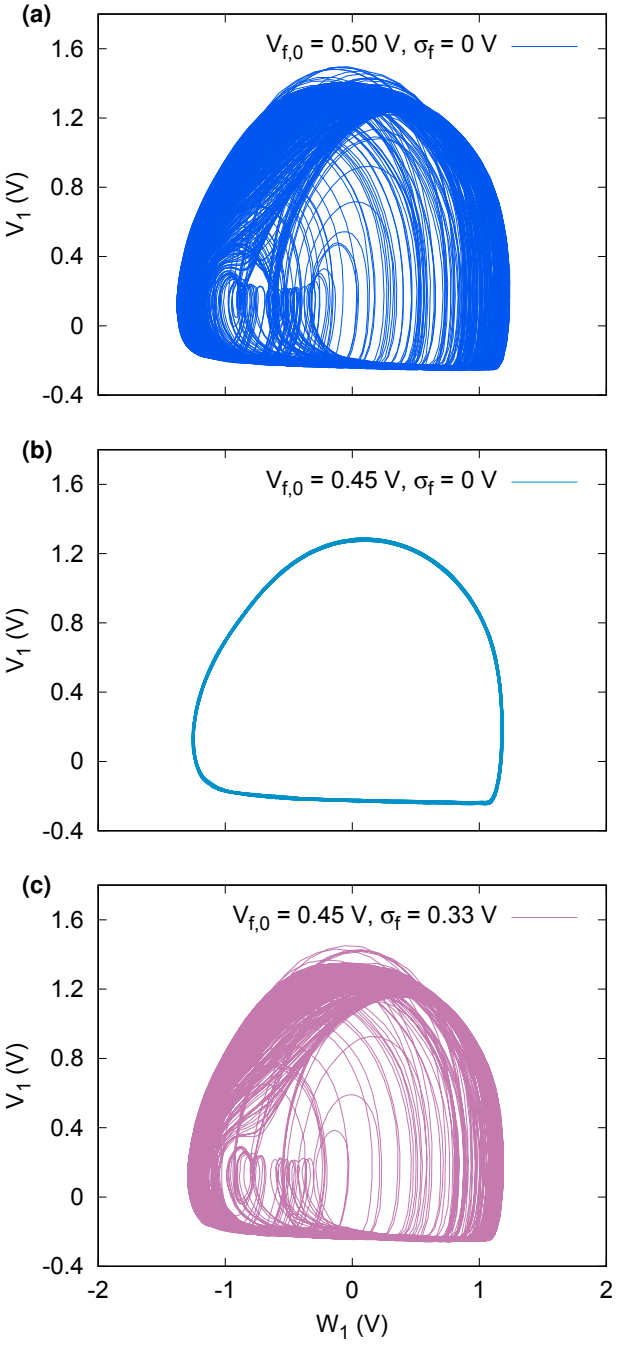

Fig. 3. State space trajectories (only the variables W_1, V_1 are plotted) corresponding to 5 s long recordings with $V_d = 0.10\,\mathrm{V}$ and for different settings of the $V_f(t)$ parameter: (a) noiseless, $V_{f,0} = 0.50\,\mathrm{V}$; (b) noiseless, $V_{f,0} = 0.45\,\mathrm{V}$; (c) noisy, $\sigma_f = 0.33\,\mathrm{V}$ and $V_{f,0} = 0.45\,\mathrm{V}$.

robust evidence of the chaotic nature of the dynamics shown in Fig. 3 (a) was provided in the work where the circuit was first proposed (Perinelli et al., 2023). Therein, chaos was experimentally demonstrated by relying on the estimation of both the attractor's correlation dimension

and its maximum Lyapunov exponent. In the same work, a theoretical assessment of the maximum Lyapunov exponent was also provided by applying the so-called standard method (Benettin et al., 1980a,b): such an assessment is here impractical due to intermittency and to the presence of a noisy term in the differential equations. Nevertheless, one can reasonably assume that the resemblance of the state space trajectories in Fig. 3 (a) and Fig. 3 (c) is reflected in a similar underlying dynamics.

The irregularity of the behavior shown in Fig. 3 (c) is better understood by looking at the time series of a single variable: an excerpt of the V_1 evolution is shown in Fig. 4. (The signal V_2 corresponding to the second block exhibits a very similar behavior). The dynamics appears to intermittently alternate between periodic orbits and irregular, chaotic regimes.

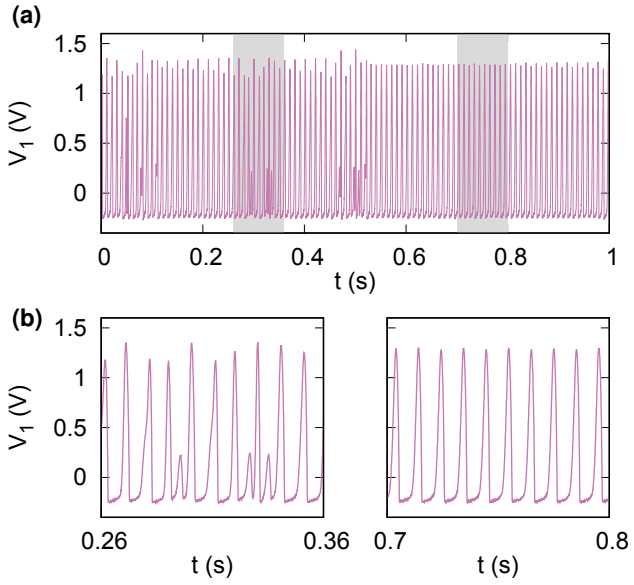

Fig. 4. Time evolution of V_1 for $\sigma_f = 0.33\,\mathrm{V}$ and $V_{f,0} = 0.45\,\mathrm{V}$, corresponding to the attractor of Fig. 3 (c). (a) Excerpt of 1 s of the V_1 evolution. (b) Segments of the V_1 evolution corresponding to the two gray shaded areas in (a) of 100 ms duration; the first segment exhibits chaos, while the second one corresponds to a periodic dynamic.

To provide a quantification of the degree of irregularity of the system and to characterize it as a function of the parameters $V_{f,0}$, σ_f, we consider the local maxima of V_1 occurring within 5 s long recordings. The approach is equivalent to the construction of a bifurcation diagram: in the case of a periodic orbit, one expects all maxima to have the same value; conversely, irregular segments provide local maxima whose amplitude is distributed between $\sim 0.1\,\mathrm{V}$ and $\sim 1.5\,\mathrm{V}$, where the latter value is close to the maxima of the periodic oscillations as highlighted in Fig. 4.

A possible quantifier of the irregularity of the dynamics is thus given by the dispersion of the values taken up by local maxima. It is convenient to exploit the natural quantization of voltage values introduced by sampling, which effectively provides a natural "binning" of V_1 maxima: because of the 12-bit effective resolution with which V_1 is sampled, the difference between two consecutive voltage values—i.e. the "bin width"—turns out to be 2.8 mV. The dispersion of maxima values can be thus estimated by simply counting the number n of unique voltage values that are taken up by the maxima.

The number n is mapped in Fig. 5 as a function of the constant voltage $V_{f,0}$ (from 0.43 V to 0.47 V in steps of 5 mV) and of the noise amplitude σ_f (from 0.01 V to 0.42 V in steps of 10 mV). In the color map, warmer hues identify

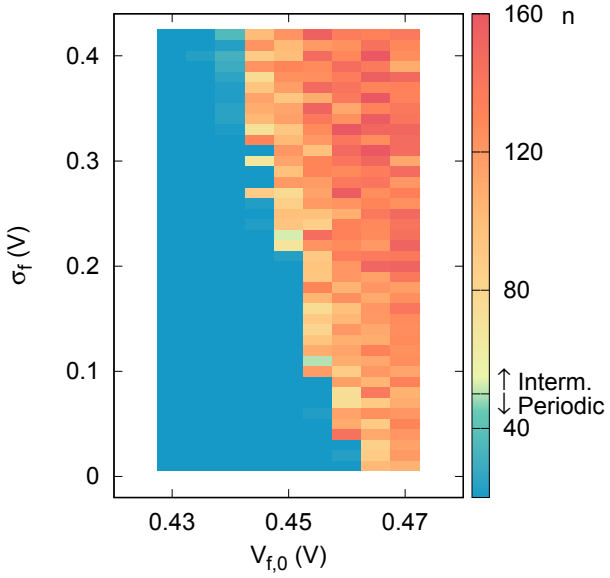

Fig. 5. Color map of the number n of unique voltage values taken up by local maxima of V_1 as a function of the parameters $V_{f,0}$, σ_f. The binning is automatically provided by the resolution of the oscilloscope. Warmer hues correspond to more irregular the dynamics. The periodic/intermittent threshold is set to $n = 50$.

irregular dynamical regimes with intermittent chaos. By visually inspecting the time series and phase portraits, we set at $n = 50$ the threshold between those that actually exhibit an intermittent regime and those that exhibit periodicity with amplitude fluctuations. Each pixel of the color map was obtained by analyzing 5 s long recordings, corresponding to $\sim 10^3$ "spikes" of the V_i voltage signal. Because intermittency corresponds to 50 - 160 different local maxima values, each pixel count would correspond, on average, to the analysis of ~ 10 independent shorter segments (of the order of 0.5 s). An improvement of the statistical size of the data contributing to each pixel could be achieved by analyzing longer recordings or, equivalently, by considering multiple acquisitions for each $V_{f,0}$, σ_f pair.

The results in Fig. 5 show that, for a range of $V_{f,0}$ values, there exist a critical noise level above which one observes intermittent chaos in the BK model. The dependence of this minimum value of σ_f on the voltage $V_{f,0}$ is quite steep: the critical noise level decreases by about 20 times the increase in $V_{f,0}$.

4. DISCUSSION

The V_f parameter of the BK model electronic analog of Fig. 2 makes up a convenient port to inject dynamical noise into the system, also considering its high input impedance. In the present work, we observed a non-trivial effect due to a noisy $V_f(t) = V_{f,0} + \sigma_f \eta(t)$, namely intermittent chaotic regimes that perturb otherwise periodic orbits. The onset of these regimes is highly sensitive to the offset $V_{f,0} = \langle V_f(t) \rangle$, as one would expect for a chaotic system. The irregular behavior is triggered above a minimum noise amplitude σ_f and persists for higher values of σ_f (at least within the range probed here). The color gradient of Fig. 5 hints at a higher irregularity—and therefore a higher frequency of occurrence of transitions to a chaotic state—for larger noise amplitudes.

An explaination of the observed behavior is not trivial, as the onset of chaotic segments occurs randomly in time. One could hypothesize a "resonance" effect in which the frequency components of injected noise close to the natural frequency of the oscillators sometimes contribute constructively, apparently leading to an increase of the constant term $V_{f,0}$. In other words, the op-amps producing W_i integrate the difference $V_d - V_i$ and, therefore, the injected noise, producing an effective low-pass filtered noise at the input of the op-amps producing V_i. Stochastic fluctuations of the injected noise towards positive or negative values for a significant fraction of the circuit's characteristic time are then propagated through this integration chain and can contribute to trigger a spike in the V_i voltage. In turn, such a noise-triggered spike perturbs a periodic orbit and might bring the system into a chaotic regime. To address this possibility, investigations with colored noise sources with frequency-dependent power spectra are called for. Two classes of noise can be particularly interesting: noise with power-law spectra (red or pink noise), which provide a long-tailed autocorrelation, and noise with a "carrier" frequency close to the circuit's characteristic frequency (i.e. noisy sinusoidals). The distribution of noise amplitudes, on the other hand, is not expected to significantly affect the dynamics as long as the noise bandwidth is much larger than the circuit's characteristic frequency. Under this condition, the central limit theorem ensures that the effective noise distribution "felt" by the circuit is approximately Gaussian.

It is also worth mentioning that the existence of intermittence between periodic and irregular motion in seismogenesis has been hypothesized out of real fault data (Shelly, 2010; Iliopoulos et al., 2012). The present work opens up a possible research strategy to address intermittency by relying on the BK model.

From the analytical point of view, valuable information is expected by the assessment of the Lyapunov exponents out of experimental time series by relying on embedding techniques (Franchi and Ricci, 2014; Perinelli and Ricci, 2018; Ricci et al., 2020). These techniques, however, should be carefully tuned to deal with the intermittency phenomenon observed here.

ACKNOWLEDGEMENTS

The authors thank the Italian Space Agency for the financial support under the contract ASI "LIMADOU Scienza+" n. 2020-31-HH.0.

REFERENCES

Analog Devices (2002). OP470 datasheet. URL `www.analog.com/media/en/technical-documentation/data-sheets/OP470.pdf`.

Benettin, G., Galgani, L., Giorgilli, A., and Strelcyn, J. (1980a). Lyapunov characteristic exponents for smooth dynamical systems and for hamiltonian systems; a method for computing all of them. part 1: Theory. *Meccanica*, 15. doi:10.1007/BF02128236.

Benettin, G., Galgani, L., Giorgilli, A., and Strelcyn, J. (1980b). Lyapunov characteristic exponents for smooth dynamical systems and for hamiltonian systems; a method for computing all of them. part 2: Numerical application. *Meccanica*, 15. doi:10.1007/BF02128237.

Bertuccio, G. (2022). On the physical origin of the electro-mechano-acoustical analogy. *J. Acoust. Soc. Am.*, 151, 2066–2076. doi:10.1121/10.0009803.

Burridge, R. and Knopoff, L. (1967). Model and theoretical seismicity. *Bull. Seismol. Soc. Amer.*, 57, 341–371. doi:10.1785/BSSA0570030341.

Carlson, J.M. (1991). Two-dimensional model of a fault. *Phys. Rev. A*, 44, 6226–6232. doi: 10.1103/PhysRevA.44.6226.

Carlson, J.M., Langer, J.S., and Shaw, B.E. (1994). Dynamics of earthquake faults. *Rev. Mod. Phys.*, 66, 657–670. doi:10.1103/RevModPhys.66.657.

Chua, L.O., Yu, J., and Yu, Y. (1985). Bipolar - JFET - MOSFET negative resistance devices. *IEEE Transactions on Circuits and Systems*, 32, 46–61. doi: 10.1109/TCS.1985.1085599.

de Sousa Vieira, M. (1999). Chaos and Synchronized Chaos in an Earthquake Model. *Phys. Rev. Lett.*, 82, 201–204. doi:10.1103/PhysRevLett.82.201.

Diodes Incorporated (2021). DFLS1100 datasheet. URL `www.diodes.com/assets/Datasheets/ds30497.pdf`.

Field, S., Venturi, N., and Nori, F. (1995). Marginal stability and chaos in coupled faults modeled by nonlinear circuits. *Phys. Rev. Lett.*, 74, 74–77. doi: 10.1103/PhysRevLett.74.74.

Franchi, M. and Ricci, L. (2014). Statistical properties of the maximum Lyapunov exponent calculated via the divergence rate method. *Phys. Rev. E*, 90, 062920. doi: 10.1103/PhysRevE.90.062920.

Iliopoulos, A.C., Pavlos, G.P., Papadimitriou, E.E., Sfiris, D.S., Athanasiou, M.A., and Tsoutsouras, V.G. (2012). Chaos, self organized criticality, intermittent turbulence and nonextensivity revealed from seismogenesis in North Aegean area. *Int. J. Bifurcat. Chaos*, 22, 1250224. doi: 10.1142/S0218127412502240.

Nakanishi, H. (1998). Complex Behavior in Earthquake Dynamics. *Int. J. Mod. Phys. B*, 12, 273–284. doi: 10.1142/S0217979298000211.

Perinelli, A., Iuppa, R., and Ricci, L. (2023). A scalable electronic analog of the burridge–knopoff model of earthquake faults. *Chaos*, 33, 093103. doi: 10.1063/5.0161339.

Perinelli, A. and Ricci, L. (2018). Identification of suitable embedding dimensions and lags for time series generated by chaotic, finite-dimensional systems. *Phys. Rev. E*, 98, 052226. doi:10.1103/PhysRevE.98.052226.

Perinelli, A. and Ricci, L. (2020). Chasing chaos by improved identification of suitable embedding dimensions and lags. *Chaos*, 30, 123104. doi:10.1063/5.0029333.

Popp, K. and Stelter, P. (1990). Stick-slip vibrations and chaos. *Philos. T. R. Soc. A.*, 332(1624), 89–105. doi: 10.1098/rsta.1990.0102.

Ricci, L., Perinelli, A., and Franchi, M. (2020). Asymptotic behavior of the time-dependent divergence exponent. *Phys. Rev. E*, 101, 042211. doi: 10.1103/PhysRevE.101.042211.

Ryabov, V.B. and Ito, H.M. (1995). Multistability and chaos in a spring-block model. *Phys. Rev. E*, 52, 6101–6112. doi:10.1103/PhysRevE.52.6101.

Shelly, D.R. (2010). Periodic, chaotic, and doubled earthquake recurrence intervals on the deep San Andreas fault. *Science*, 328, 1385–1388. doi: 10.1126/science.1189741.